Nuclear factor-κB p65 small interfering RNA or proteasome inhibitor bortezomib sensitizes head and neck squamous cell carcinomas to classic histone deacetylase inhibitors and novel histone deacetylase inhibitor PXD101

Jianming Duan,[1] Jay Friedman,[1] Liesl Nottingham,[1] Zhong Chen,[1] Gulshan Ara,[2] and Carter Van Waes[1]

[1]Tumor Biology Section, Head and Neck Surgery Branch, National Institute on Deafness and Other Communication Disorders, NIH, Bethesda, Maryland and [2]CuraGen Corp., Branford, Connecticut

Abstract

Histone deacetylase inhibitors (HDI) can inhibit proliferation and enhance apoptosis in a wide range of malignancies. However, HDIs show relatively modest activity in head and neck squamous cell carcinomas (HNSCC), in which we have shown the activation of nuclear factor-κB (NF-κB; NF-κB1/RelA or p50/p65), a transcription factor that promotes expression of proliferative and antiapoptotic genes. In this study, we examined if HDIs enhance activation of NF-κB and target genes and if genetic or pharmacologic inhibition of NF-κB can sensitize HNSCC to HDIs. Limited activity of classic HDIs trichostatin A and sodium butyrate was associated with enhanced activation of NF-κB reporter activity in a panel of six HNSCC cell lines. HDIs enhanced NF-κB p50/p65 DNA binding and acetylation of the RelA p65 subunit. Transfection of small interfering RNAs targeting p65 strongly inhibited NF-κB expression and activation, induced cell cycle arrest and cell death, and further sensitized HNSCC cells when combined with HDIs. The p65 small interfering RNA inhibited HDI-enhanced expression of several NF-κB–inducible genes implicated in oncogenesis of HNSCC, such as *p21, cyclin D1*, and *BCL-XL*. Bortezomib, an inhibitor of proteasome-dependent NF-κB activation, also increased sensitization to trichostatin A, sodium butyrate, and a novel HDI, PXD101, *in vitro*, and to the antitumor effects of PXD101 in bortezomib-resistant UMSCC-11A xenografts. However, gastrointestinal toxicity, weight loss, and mortality of the combination were dose limiting and required parenteral fluid administration. We conclude that HDI-enhanced NF-κB activation is one of the major mechanisms of resistance of HNSCC to HDIs. The combination of HDI and proteasome inhibitor produced increased antitumor activity. Low starting dosages for clinical studies combining HDIs with proteasome inhibitors and IV fluid support may be warranted. [Mol Cancer Ther 2007;6(1):37–50]

Introduction

Head and neck squamous cell carcinomas (HNSCC), which arise from the mucosal epithelial lining of the upper aerodigestive tract, account for ~40,000 new cases and ~12,000 cancer deaths in the United States and 500,000 deaths worldwide annually (1). Despite advances in treatment by surgery, radiation, and chemotherapy, approximately half of patients with HNSCC still die within 5 years, and many of the ~300,000 surviving patients suffer significant impairment in voice, speech, and swallowing as a result of cancer or treatment. Consequently, there has been considerable interest in identifying new molecularly targeted agents that have greater and more selective activity for HNSCC.

Histone deacetylase (HDAC) inhibitors (HDI) represent an important class of agents with anticancer activity. Treatment with HDIs causes the accumulation of acetylated histones and other proteins regulating chromatin structure and transcription, thereby altering the transactivation and expression of specific genes that regulate cell growth arrest, differentiation, or apoptosis (2). The HDIs include the classic hydroxamic acid, trichostatin A (TSA), and butyrate, sodium butyrate (NaBu), and newer synthetics with more favorable pharmacologic characteristics for therapeutic investigation (3–5). Among these, phenylbutyrate, depsipeptide, SAHA, MS275, and PXD101 have been investigated in preclinical and early-phase clinical trials. In preclinical studies, HDIs have shown variable antiproliferative and cytotoxic activity in a wide range of solid malignancies, including head and neck, breast, colon, lung, and ovarian cancers as well as hematologic malignancies, such as lymphomas, leukemias, and myeloma (3–5). In clinical trials, monotherapy with HDIs has mostly produced partial responses, whereas various combinations are under investigation to increase activity. In HNSCC, classic HDIs have shown modest antiproliferative and cytotoxic activity when used alone (6, 7) and greater activity when

Received 7/27/06; revised 11/8/06; accepted 11/20/06.

Grant support: National Institute on Deafness and Other Communication Disorders Intramural Project Z01-DC00016.

The costs of publication of this article were defrayed in part by the payment of page charges. This article must therefore be hereby marked *advertisement* in accordance with 18 U.S.C. Section 1734 solely to indicate this fact.

Note: J. Duan and J. Friedman contributed equally as first authors to experimental work.

Requests for reprints: Carter Van Waes, National Institute on Deafness and Other Communication Disorders, NIH, CRC Building 10, Room 4-2732, 10 Center Drive, Bethesda, MD 20892. Phone: 301-402-4216; Fax: 301-402-1140. E-mail: vanwaesc@nidcd.nih.gov

doi:10.1158/1535-7163.MCT-05-0285

used in combination with radiation and demethylating agents (8, 9). The basis for the limited sensitivity of HNSCC and other cancers to cytotoxic effects of HDIs is not well understood, and greater understanding of the possible mechanisms is needed to guide the investigation of rationale combinations.

We have identified previously a molecular mechanism that could potentially contribute to the relative resistance of HNSCC and other malignancies to cytotoxic effects of HDIs. We showed that a signal transcription factor, nuclear factor-κB (NF-κB; NF-κB1/RelA p50/p65), is constitutively activated in human and murine SCC (10–12). Because activation of the NF-κB heterodimer involves signal phosphorylation, ubiquitination, and proteasome-dependent degradation of an inhibitor-κB protein, IκBα (13), we examined the effects of blocking NF-κB activation by expression of a dominant-negative IκBα phosphorylation site mutant (IκBαM) or proteasome inhibitor, which block IκB degradation. Genetic inhibition of NF-κB was found to restore the expression of many genes differentially expressed by SCC to levels detected in normal keratinocytes and inhibit malignant phenotypic features, including cell survival, proliferation, migration, angiogenesis, and tumorigenesis (11, 12). Similarly, a proteasome inhibitor, bortezomib, inhibited NF-κB and had cytotoxic, antiangiogenic activity, partially inhibiting HNSCC tumor growth in preclinical and clinical studies (14). Inhibition of NF-κB was shown to sensitize HNSCC to effects of tumor necrosis factor and radiation, indicating that it can promote resistance to cytotoxic therapies (15–17).

Regulation of NF-κB1/RelA DNA binding, transactivation, and turnover has been shown to involve acetylation of RelA p65 by histone acetylase CBP/p300 and deacetylation by HDACs (18, 19). Exposure to HDIs has been shown to enhance acetylation of p65 and activation of NF-κB (18). Given the role of NF-κB1/RelA in prosurvival mechanisms in HNSCC, we hypothesized that the relative resistance of HNSCC to HDIs could result from the enhanced activation and acetylation of NF-κB, and expression of NF-κB regulated genes known to promote cell survival. In this study, we examined if classic HDIs TSA and NaBu enhance basal transactivation, DNA binding and acetylation of NF-κB p65, and expression of NF-κB–regulated proliferative and antiapoptotic genes. We determined if specific NF-κB inhibition by p65 small interfering RNA (siRNA) blocks activation of NF-κB and these genes and sensitizes HNSCC to these HDIs. We examined the cytotoxic effects of combining classic HDIs and a novel HDI, PXD101, with proteasome inhibitor bortezomib *in vitro* as well as antitumor and systemic effects of combining PXD101 with bortezomib in mice bearing human HNSCC xenografts *in vivo*.

Materials and Methods

Inhibitors and Antibodies

Classic HDIs TSA and NaBu were purchased from Sigma-Aldrich (St. Louis, MO). The IC_{50}s for inhibition of growth of most tumor cell lines range from 0.040 to 0.070 μmol/L TSA and 1,500 μmol/L NaBu (20, 21). The stock solution for TSA was reconstituted in DMSO at a concentration of 1 mmol/L, stored at −20°C, and diluted into complete cell culture medium before use. The stock solution for NaBu was prepared in double-distilled H_2O at a concentration of 1 mol/L, stored at −20°C, and diluted into complete cell culture medium before use.

PXD101 is a novel hydroxamate class HDI that inhibits HDAC activity with IC_{50}s of 0.009 to 0.1 μmol/L and enhances histone acetylation and cytoxicity in tumor cells with IC_{50}s in the range of 0.2 to 5 μmol/L (22). PXD101 has also been shown to achieve serum concentrations in or above these ranges and to partially inhibit growth of human ovarian and colon carcinoma xenografts with minimal toxicity in mice when given daily i.p up to 40 mg/kg (22). Bortezomib (Velcade, formerly PS-341) is a first-in-class proteasome inhibitor (23) that inhibits NF-κB in HNSCC lines *in vitro* and tumor in xenografts and patients *in vivo* (14, 17, 24). PXD101 was provided by TopoTarget and CuraGen (Branford, CT), and bortezomib was provided by Millennium Pharmaceuticals (Cambridge, MA) under Materials Cooperative Research and Development Agreements. PXD101 was prepared with L-arginine in PBS, and bortezomib was prepared in aqueous solution according to the manufacturer's instructions.

Antibodies used in these studies purchased from Santa Cruz Biotechnology (Santa Cruz, CA) included NF-κB p65 (FC-6) and NF-κB p65/p50 (C-19) AC for immunoprecipitation, pan-acetyl (C2) for acetylation analysis, and NF-κB p65 (A) and NF-κB p65/p50 (H-119), goat anti-mouse IgG–horseradish peroxidase, and goat anti-rabbit IgG–horseradish peroxidase as the secondary antibodies for Western blot analysis. For detection of p65 after siRNA knockdown, Western blot was done using anti-p65, β-actin primary, and antirabbit horseradish peroxidase–linked secondary antibodies (Cell Signaling Technology, Danvers, MA).

Cell Culture

Human HNSCC cell lines UMSCC-1, UMSCC-6, UMSCC-9, UMSCC-11A, UMSCC-11B, and UMSCC-38 from University of Michigan UMSCC series (25) were kindly provided by Dr. T.E. Carey (University of Michigan, Ann Arbor, MI). These cell lines have been extensively characterized and exhibit alterations detected in the majority of HNSCC, including epidermal growth factor receptor activation (26), constitutive activation of NF-κB and target genes (10–12) and either wild-type (UMSCC-1, UMSCC-6, UMSCC-9, and UMSCC-11A) or mutant (UMSCC-11B and UMSCC-38) p53 genotype (27).[3] UMSCC-11A and UMSCC-11B were used for molecular studies because they have been shown previously to form xenografts and differ in sensitivity to chemotherapy agents, with UMSCC-11A being relatively more resistant

[3] T.L. Lee, unpublished data.

to bortezomib and other agents *in vitro* and in mice *in vivo* (16).[4] The cell lines were maintained in Eagle's MEM supplemented with 10% FCS, 1% glutamine, and 0.5% penicillin/streptomycin at 37°C in 5% CO_2.

HDAC Activity Assay

HDAC activity was analyzed before and after TSA (0.2 μmol/L) and NaBu (500 μmol/L) treatment using the HDAC kit from Biomol (Plymouth Meeting, PA) as directed by the manufacturer.

Transfection with siRNA

SMARTpool p65 (RelA) siRNAs consist of four double-stranded siRNAs commercially designed and tested by Dharmacon, Inc. (Dallas, TX). The pool of siRNAs contained the p65-specific sequences GATGAGATCTTCCTACTGT, CAAGATCAATGGCTACACA, GGATTGAGGAGAAACGTAA, and CTCAAGATCTGCCGAGTGA. Control (nonsilencing) siRNA (Qiagen, Germantown, MD) was used as the negative control and its sequence AATTCTCCGAACGTGTCACGT was analyzed in a BLAST search to exclude homology to p65 or other genes. UMSCC-11A and UMSCC-11B cells at 50% to 70% were transfected with p65 (RelA) SMARTpool siRNAs (100 nmol/L) or control siRNA (100 nmol/L) by LipofectAMINE 2000 (Invitrogen, Carlsbad, CA) for 5 h at 37°C in six-well culture plates or 100-mm tissue culture plates in Opti-MEM (Invitrogen). Following transfection, cells were grown in complete MEM and treated or collected as indicated.

3-(4,5-Dimethylthiazol-2-yl)-2,5-Diphenyltetrazolium Bromide Cell Proliferation Assay

UMSCC cells (5×10^3 per well) were grown in 96-well plates and exposed to TSA, NaBu, PXD101, bortezomib, or combination of these reagents, 24 h after the cells were plated. Cell proliferation and viability were measured daily for up to 5 consecutive days using a 3-(4,5-dimethylthiazol-2-yl)-2,5-diphenyltetrazolium bromide (MTT) cell proliferation kit (Roche Diagnostics, Indianapolis, IN). Absorbance at 570 nm was determined using a microtiter ELISA plate reader (Biotek Instruments, Inc., Winooski, VT).

Proliferation of UMSCC-11A and UMSCC-11B cell lines transfected with p65 (RelA) siRNAs was also measured using the MTT cell proliferation kit. Cells were transfected with p65 siRNA, nonsilencing siRNA, or no oligonucleotide as controls in six-well plates for 24 h, trypsinized, and transferred as six replicates to a 96-well, flat-bottomed plate at a concentration of 5×10^3 cells per well in 100 μL of complete MEM with or without TSA and NaBu. Cells were incubated at 37°C in 5% CO_2 for 1, 3, or 5 days, and growth rates were analyzed by MTT as described above.

Apoptosis Assay

UMSCC-11A and UMSCC-11B cells (5×10^3 per well) were grown in 96-well plates and exposed to HDIs. After 24 h, cells were harvested, and the extent of apoptosis was determined by quantitation of nucleosomes released into the cytoplasm using the Cell Death Detection ELISA Plus kit (Roche Applied Science, Indianapolis, IN) according to the manufacturer's directions. The assay has been standardized against DNA laddering, a hallmark of apoptosis (28, 29).

Transcription Factor Binding and Electrophoretic Mobility Shift Assays

UMSCC-11A and UMSCC-11B cells (5×10^4 per plate) were plated into 100-mm plates and exposed to HDIs. Nuclear extracts were harvested using Nuclear Extract kit (Active Motif, Carlsbad, CA) at the desired time points following the manufacturer's instruction. Five micrograms of nuclear extracts for each sample were used to quantify the NF-κB activation by the binding of p65 and p50 with TransAM Transcription Factor Assay kit (Active Motif).

The DNA binding activity of NF-κB was further confirmed with biotin-labeled oligonucleotide NF-κB probe (5′-AGTTGAGGGGACTTTCCCAGGC-3′) using an electrophoretic mobility shift assay kit according to the manufacturer's instructions (Panomics, Inc., Redwood City, CA; refs. 30, 31). Five micrograms of nuclear protein were incubated for 30 min at 21°C with biotinylated NF-κB probe. To test the specificity of the binding, 3 μL unlabeled probe was added to compete with the labeled probe. For supershift assay, 1 μL of the appropriate antibodies was added to the nuclear extracts for 20 min at room temperature before the addition of the labeled probe. The DNA binding activity of ornithine carbamyl transferase-1 was assessed as loading control. Samples were run on 6% DNA retardation gel (Invitrogen) at 120 V for 2 h, then transferred to nylon membrane, and subjected UV cross-linking and autoradiography according to the manufacturer's instruction.

Reporter Gene Assay

The p65-Luc and pRSV-LacZ plasmids were cotransfected as described previously (26) or combined with p65 siRNA or control siRNA following the procedure described above. The cells were harvested at 24 to 48 h after transfection, and the reporter gene activities were assayed using the Dual-Light Combined Reporter Gene Assay System for detection of luciferase and β-galactosidase (Tropix, Bedford, MA). The relative light units were calculated as follows: relative light units = (light units from luciferase) / (light units from β-galactosidase).

Cell Cycle Analysis

UMSCC-11A and UMSCC-11B cells treated with different HDIs were incubated for times indicated before harvesting. Both live monolayer cells and dead nonadhesive cells were collected and counted by hemocytometer using trypan blue solution (Invitrogen). The cells were stained with propidium iodide provided by Cycletest Plus DNA Reagent kit (Becton Dickinson, San Jose, CA) following the manufacturer's suggestions. DNA staining was quantified by FACScan flow cytometer (Becton Dickinson) using CellQuest software (Becton Dickinson). Cell cycle and DNA degradation of cells were analyzed by ModFit LT software (Verity Software House, Inc., Topsham, MA).

[4] Z. Chen, unpublished data.

RNA Isolation, Reverse Transcription, and Real-time Quantitative PCR

Total RNA was isolated from cultured UMSCC-11A and UMSCC-11B cells using Trizol reagent (Invitrogen) and purified with RNeasy column (Qiagen, Valencia, CA). Ten micrograms of purified total RNA were used for a reverse transcription reaction using Applied Biosytems High-Capacity cDNA Archive kit (Applied Biosystems). The real-time quantitative PCR was done using above-generated cDNA samples with Taqman Assays-on-Demand primers and kit (Applied Biosystems). The assay ID numbers for the primer pairs and probes used were RelA (Hs00153294), cyclin D1 (Hs00277039), BIRC2/inhibitor of apoptosis 1 (IAP1; Hs00357350), BCL-XL (Hs00236329), p21/WAF1 (Hs00355782), and glyceraldehyde-3-phosphate dehydrogenase (GAPDH; Hs9999905; Applied Biosystems). Each assay was run in triplicate. A linear regression was done for each primer set to calculate the amount of starting material in each sample. All samples were normalized to GAPDH. A comparison was done for each sample using a relative cycle threshold (C_t) comparison. An average C_t was calculated for the triplicate reactions and normalized to GAPDH ($\Delta C_t = C_{t\ \text{Sample}} - C_{t\ \text{GAPDH}}$). The C_ts were then compared between different treatments and time points ($\Delta\Delta C_t$) with normalization to the untreated samples. Finally, a fold change was calculated from the $\Delta\Delta C_t$ (fold change = $2^{\Delta\Delta Ct}$).

Immunoprecipitations and Western Blot Analysis

The extracts of indicated cell lines were harvested before and after various treatments using Nuclear Extract kit at the desired time points following the manufacturer's instruction. Fifteen micrograms of nuclear extracts for each sample were incubated with 20 μL indicated agarose-conjugated primary antibody at 4°C overnight. The immunoprecipitates were collected by centrifugation at 1,000 × *g* for 30 s at 4°C and the beads were washed for four times with PBS buffer. The beads were then resuspended in 20 μL of 2× SDS sample buffer, boiled for 3 min, and analyzed on NuPAGE (Invitrogen). Proteins were transferred to nitrocellulose polyvinylidene difluoride membranes (Invitrogen), blocked with 5% milk in TBST [20 mmol/L Tris-HCl (pH 7.6), 137 mmol/L NaCl, 0.5% Tween 20], and incubated with the indicated antibodies for 60 min. Membranes were then washed with TBST and incubated for 60 min with secondary antibody, washed with TBST, and incubated with enhanced chemiluminescence reagent (Amersham, Piscataway, NJ). Membranes were exposed to X-ray film to visualize the bands.

Animal Studies

Immunodeficient BALB/c SCID mice were obtained from the National Cancer Institute, Frederick Cancer Research and Development Center, Animal Production Area. The animals were housed in a specific pathogen-free animal facility. Animal care was provided under a NIH Animal Care and Use Committee–approved protocol (1226-05). Tumors were established by injecting 5×10^6 UMSCC-11A cells s.c. into the left flank of BALB/c SCID mice (7 weeks of age, male, and weight of 20–25 g). When tumors were palpable on day 11, animals were randomized into groups of eight and i.p. injection of drugs using sterile technique commenced. Bortezomib was dissolved in sterile normal saline and given at a dose of 0.8 mg/kg at intervals indicated. PXD101 stock solution (50 mg/mL) was prepared in a L-arginine solution (final concentration of L-arginine was 520 mmol/L) and filtered. PXD101 (50 mg/mL) was diluted with sterile PBS and given at a dose of 60 mg/kg at times specified. Three times weekly, tumors were independently measured bidimensionally by a staff technician and tumor volumes were calculated as volume (cm^3) = ($L \times W^2$) / 2. Body weights and appearance were also monitored, and 2.0 mL saline s.c. was given to mice showing evidence of diarrhea and/or weight loss, which was observed in pilot experiments.

Statistical Analysis

The data obtained are expressed as mean ± SD. Statistical evaluation of data was done with two-tailed Student's *t* test. *P* values <0.05 were considered statistically significant.

Results

Limited Inhibitory Effects of HDIs in UMSCC Cells with Basal and HDI-Inducible Activation of NF-κB Activity

HDIs have been reported to inhibit proliferation and/or induce cell death of eukaryotic cells *in vitro* and *in vivo* (20, 21). To examine the sensitivity of HNSCC to HDIs, we examined a panel of six HNSCC lines from the University of Michigan series (UMSCC). The UMSCC-1, UMSCC-6, UMSCC-9, UMSCC-11A, UMSCC-11B, and UMSCC-38 cell lines have previously been extensively characterized and found to exhibit varying levels of constitutive NF-κB activation (10, 30), consistent with variation observed in tumor specimens from patients (31). NF-κB DNA binding and luciferase activity in UMSCC-1, UMSCC-6, UMSCC-11A, and UMSCC-11B is 1- to 3-fold greater than that of UMSCC-9 and UMSCC-38 (30). The drug sensitivity of cell lines to various concentrations of TSA (0.1, 0.2, 0.5, and 1.0 μmol/L) and NaBu (200, 500, 1,000, and 2,000 μmol/L) was examined using MTT assay at 0-, 1-, 3-, and 5-day time points. Figure 1 shows results from day 3, when optimal growth and inhibition was observed. Statistically significant inhibition was detectable in most cell lines beginning with TSA above 0.2 μmol/L and NaBu above 1,000 μmol/L ($P < 0.05$; Fig. 1A). However, inhibition exceeding the IC_{50} was not observed in most of the UMSCC cell lines at concentrations of 0.5 μmol/L TSA or 2,000 μmol/L NaBu (Fig. 1A), concentrations above those reported to induce apoptosis in other cancer cell lines (0.040–0.070 μmol/L TSA; 1,500 μmol/L NaBu; refs. 20, 21). We confirmed that the inhibitors significantly inhibited HDAC activity in the different cell lines, at concentrations of 0.20 μmol/L TSA and 500 μmol/L NaBu, which were below those that inhibited cell growth (Fig. 1B). When we examined the effects of HDIs on NF-κB (Fig. 1C), we found that the HDIs significantly enhanced the basal NF-κB reporter gene activity in the cell lines at concentration(s) that inhibited

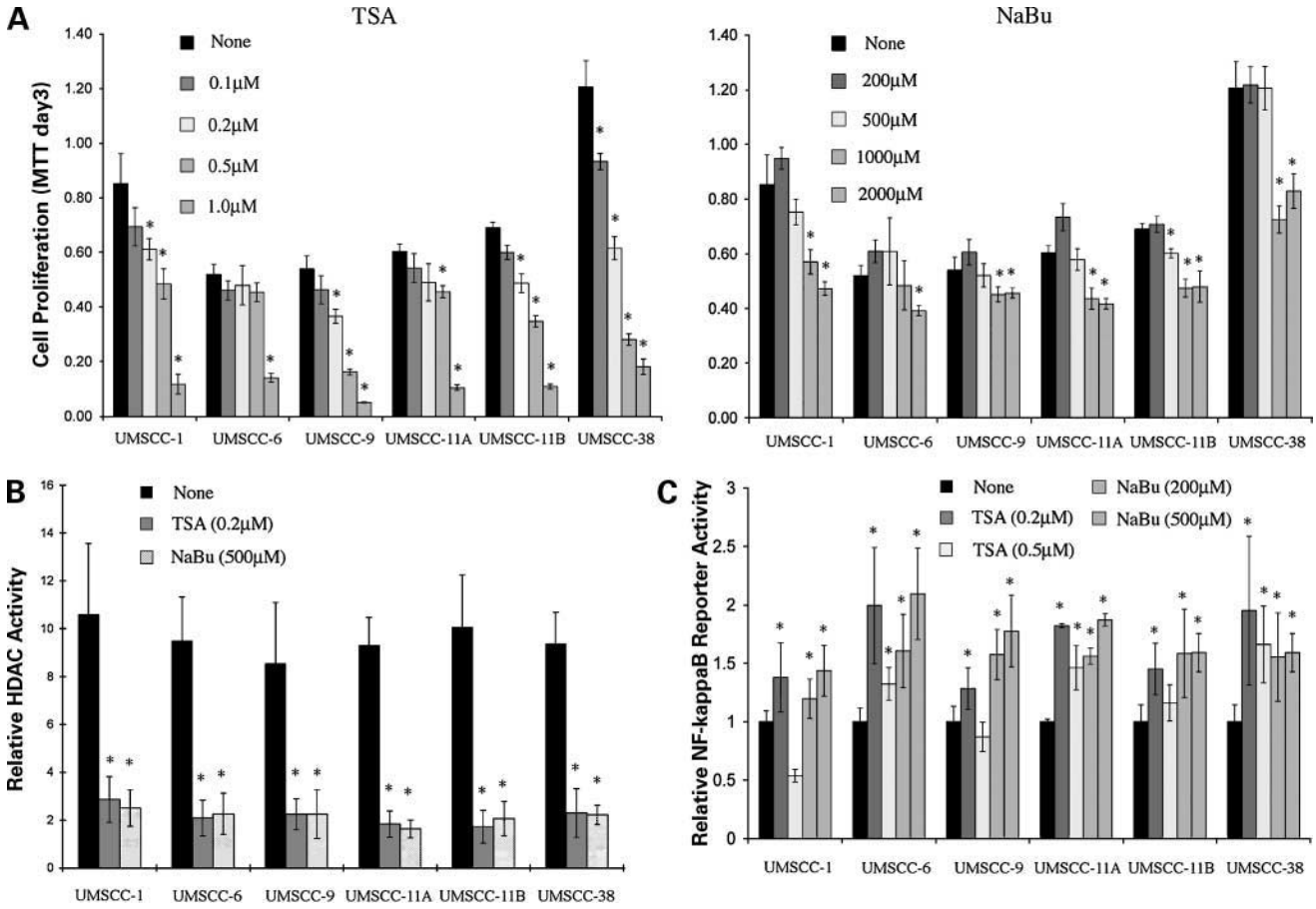

Figure 1. Limited sensitivity of UMSCC cells to HDIs is associated with HDI-induced enhancement of constitutive NF-κB reporter gene activity. **A,** 5-d MTT assay was done to test the drug sensitivity of UMSCC-1, UMSCC-6, UMSCC-9, UMSCC-11A, UMSCC-11B, and UMSCC-38 cell lines to TSA and NaBu. Results from day 3 when the optimal growth and inhibition were observed are shown. The cell density (absorbance) of cultures was measured by a microtiter ELISA reader at a wavelength of 550 nm with reference wavelength at 690 nm. Results include data from six replicate cultures. *Columns,* mean of one of two independent experiments yielding similar results; *bars,* SD. **B,** HDAC activity was analyzed before and after TSA (0.2 μmol/L) and NaBu (500 μmol/L) treatment as described in Materials and Methods. Results include pooled data from triplicate cultures from two independent experiments. *Columns,* mean; *bars,* SD. **C,** NF-κB reporter gene activity assay was done by transfection of NF-κB p65-Luc and pRSV-LacZ plasmids. TSA and NaBu were added after 24 h and the cells were harvested at 48 h. The reporter gene activities were assayed using the Dual-Light Luciferase and β-Galactosidase system. Results include pooled data from triplicate cultures from two independent experiments. *Columns,* mean; *bars,* SD. *, $P < 0.05$.

HDAC activity. Because we have shown previously that NF-κB can promote cell survival and therapeutic resistance in these UMSCC lines (15–17), these results were consistent with the possibility that constitutive and/or inducible NF-κB activation could contribute to cell survival of these cells when treated with HDIs.

HDIs Increase NF-κB p50/p65 DNA Binding and Acetylation of p65

To determine the mechanism of HDI-inducible NF-κB reporter activity in Fig. 1C above, we examined if HDIs increased nuclear DNA binding activity and acetylation of NF-κB1/RelA p50/p65, the species of NF-κB detected previously in HNSCC cell lines (10) and tumor specimens (24, 31). The UMSCC-11A and UMSCC-11B cell lines selected for further molecular analysis were shown previously to exhibit DNA binding activity composed of p50/p65 heterodimers (10) and intermediate levels of NF-κB activation among the UMSCC lines (30). These cell lines also form murine xenografts although differing in sensitivity to proteasome inhibitors despite an isogenic origin (14). Consistent with Fig. 1C, we found that HDIs induced a significant increase in DNA binding activity of p65 and p50 in both UMSCC-11A and UMSCC-11B cells, as detected by quantitative DNA binding assay (Fig. 2A). The specificity of DNA binding was further confirmed by DNA electrophoretic mobility shift assay, which showed competitive inhibition with unlabeled probe, and supershift of p65 and p50 by anti-p65 and anti-p50 antibodies (Fig. 2B). The Western blot analysis shown in Fig. 2C reveals that treatment of UMSCC-11A with both TSA and NaBu resulted in detection of increased acetylation of p65 when compared with untreated control. No significant change in total p65 protein or β-actin control was observed. No acetylation of p50 was detected by Western blot when p50

was immunoprecipitated (data not shown). Therefore, these results indicate that the activation of NF-κB by HDIs occurs with increased p65/p50 DNA binding and acetylation of p65.

Inhibition of NF-κB Activation by p65 siRNA

Based on the effect of HDIs on activation of p50/p65 and acetylation of p65, we next examined if specific inhibition of p65 expression could attenuate constitutive and HDI-induced activation of NF-κB and sensitize HNSCC to antiproliferative or cytotoxic effects of HDIs. To block p65 (RelA) expression, p65 (RelA)–specific or control double-stranded siRNAs were transfected into UMSCC-11A and UMSCC-11B cells, and p65 and GAPDH expression were quantitatively compared by real-time reverse transcription-PCR. The mRNA level of p65 was significantly decreased by >90% by p65 siRNA relative to control ($P < 0.05$) as shown in Fig. 3A. Significant suppression of RelA mRNA expression levels by p65 siRNA compared with baseline was sustained over 24 h ($P < 0.05$; Fig. 3B) but neither were significantly affected by exposure to TSA, indicating that HDIs do not modulate baseline or overcome p65 siRNA–suppressed RelA mRNA expression. A corresponding decrease in p65 protein was confirmed by Western blot (Fig. 3C). No inhibition in GAPDH mRNA or β-actin protein expression to which the results were compared was observed, making it unlikely that such reduction was due to nonspecific mechanisms (Fig. 3A and C). Both constitutive and HDI-induced DNA binding activity of p65 and p50 were significantly inhibited by p65 siRNA as shown in Fig. 3D. NF-κB p65 binding activity was decreased by >80%, whereas p50 activity was decreased by >50%. Thus, p65 siRNA inhibited both p65 mRNA and protein expression, and DNA binding of p65/p50 protein-containing NF-κB complexes in both control- and HDI-treated cells.

Inhibition of NF-κB by p65 siRNA Sensitizes HNSCC Cells to HDIs

We examined the effects of p65 siRNA knockdown above on HDI sensitivity of UMSCC-11A and UMSCC-11B cells. UMSCC-11A and UMSCC-11B cells were transfected with p65 siRNA and treated with TSA and NaBu. Figure 4A confirms that TSA and NaBu at the concentrations used had weak inhibitory effects on cell density when added with no oligonucleotide or when combined with control siRNA oligonucleotides. The siRNA targeting p65 siRNA alone significantly inhibited cell density of UMSCC-11A and UMSCC-11B cells when compared with controls ($P < 0.05$). The strongest inhibition was observed when p65 siRNA interference and HDIs were combined. Figure 4B shows corresponding effects on cell morphology in UMSCC-11A. HDIs alone had minimal affects on the morphology of cells or colonies. When compared with no oligonucleotide and nonspecific oligonucleotide controls,

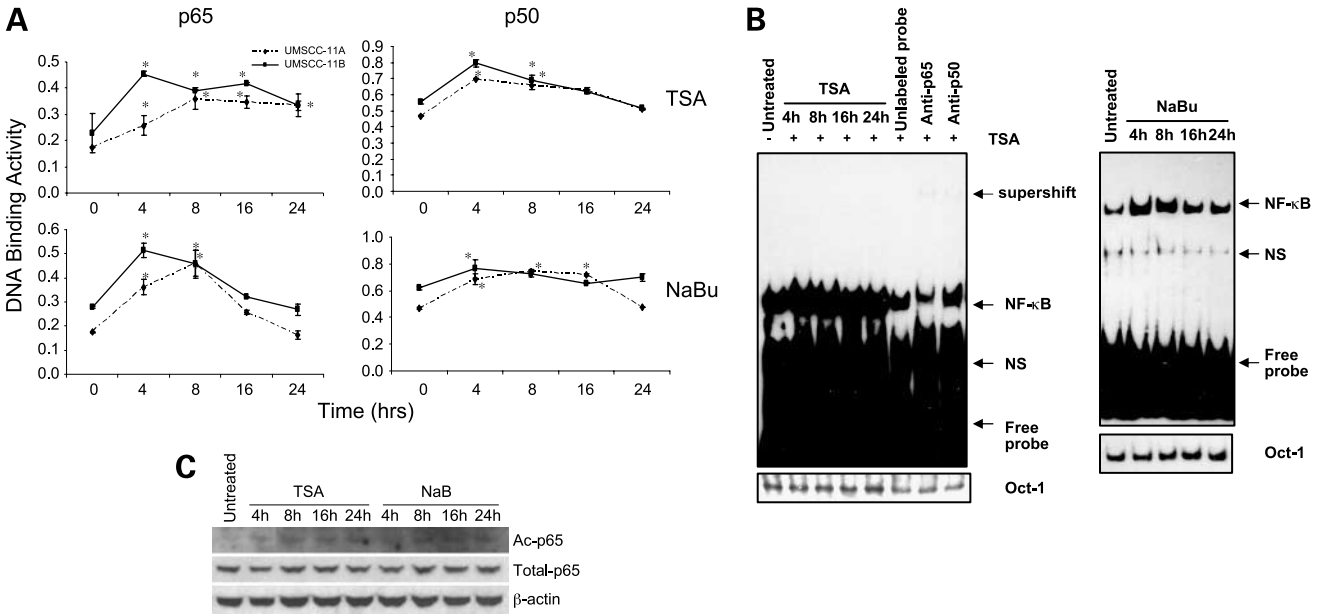

Figure 2. HDIs increase p65/p50 DNA binding and acetylation of NF-κB p65 in HNSCC. **A,** p65/p50 DNA binding was measured by ELISA-based DNA binding assay as described in Materials and Methods. UMSCC-11A and UMSCC-11B cells were plated into 100-mm plates (5×10^4 per plate) and exposed to HDIs (0.2 μmol/L TSA and 500 μmol/L NaBu). Five micrograms of nuclear extracts generated from untreated and HDI-treated UMSCC-11 cells were subjected to DNA binding assay for p65 and p50 subunits. *Points,* mean of triplicate samples from two independent experiments; *bars,* SD. *, $P < 0.05$. **B,** electrophoretic mobility shift assay was done to determine the specificity of inducible NF-κB p65/p50 DNA binding activity. Fifteen micrograms of nuclear extracts generated from untreated and TSA-treated (200 nmol/L) UMSCC-11A cells were subjected to electrophoresis on 6% of DNA retardation gel. Competition and supershift assays were done by adding the unlabeled probe and specific antibodies into the sample during probe labeling. **C,** HDIs enhance accumulation of acetylated p65. UMSCC-11A cells were treated with TSA (0.2 μmol/L) and NaBu (500 μmol/L), and nuclear extracts were subjected to immunoprecipitation with anti-p65 antibody, electrophoresis, and Western blot. The blots were probed for acetylated and total p65 proteins, and β-actin was used as the loading control.

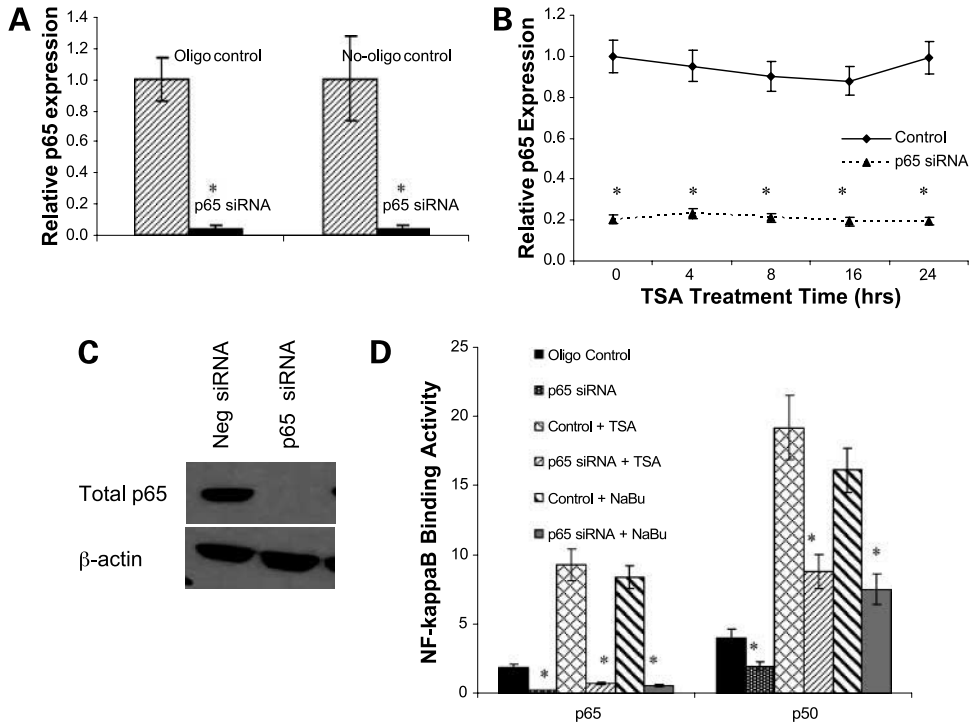

Figure 3. p65 siRNA inhibits p65 expression and NF-κB activation. **A,** *p65* gene expression was measured using real-time reverse transcription-PCR. Forty-eight hours after transfection without oligonucleotide (*Oligo*), with oligonucleotide control, or with p65 siRNA. GAPDH was used as the internal control and did not vary significantly between treatments. **B,** time course showing stability of p65 mRNA expression with and without TSA. mRNA expression was measured at intervals for 24 h in p65 siRNA – transfected and nonspecific oligonucleotide control cell cultures before (0 h) and after TSA (0.2 μmol/L) treatment by real-time reverse transcription-PCR. GAPDH was used as the internal control. **C,** Western blot showing p65 siRNA knockdown of RelA but not β-actin. UMSCC-11A protein extracts obtained 48 h after transfection with control oligonucleotide or with p65 siRNA were separated by SDS-PAGE, transferred, and developed with anti-p65 – and β-actin – specific antibodies. **D,** constitutive and HDI-induced DNA binding activity of both p65 and p50 was measured by ELISA-based TransAM assay. UMSCC-11A cells were transfected with p65 siRNA or nonspecific oligonucleotide control and treated with TSA (0.2 μmol/L) or NaBu (500 μmol/L). Data represent a result of triplicate samples from two independent experiments. *, $P < 0.05$.

treatment with p65 siRNA alone resulted in a decrease in density as well as cell rounding and blebbing. The effects on density and cell fragmentation observed with p65 siRNA alone were markedly enhanced in the presence of TSA or NaBu, consistent with massive cell death. Similar effects were shown in UMSCC-11B cells (data not shown).

To confirm whether the inhibitory and morphologic effects of HDIs and p65 siRNA were due to growth arrest and/or apoptosis, DNA cell cycle analysis and fragmentation assays were done. Fig. 5A shows DNA cell cycle histograms of UMSCC-11A cells 24 and 48 h after treatment with the HDIs, with p65 siRNA or oligonucleotide control or the combinations. The HDIs (TSA > NaBu) induced an increase in cells arrested in G_0-G_1 before S phase, with no or a minimal increase in the apoptotic sub–G_0-G_1 DNA fraction. Following transfection by p65 siRNA, there was an increase in cells in G_2-M phase arrest and small increase in the apoptotic sub–G_0-G_1 fraction from 24 to 48 h. Combining HDIs with p65 siRNA markedly increased the sub–G_0-G_1 DNA fraction by 48 h, consistent with morphologic evidence for apoptosis in Fig. 4B. Effects on the apoptotic fraction of even greater magnitude were observed in UMSCC-11B cells with the combination treatment (p65 siRNA and TSA, 43%; NaBu, 32.6%) versus control oligonucleotide (9.0%) or p65 siRNA (12.4%) alone (histograms not shown). As another independent indicator of apoptosis, we did a DNA fragmentation assay validated against standard DNA laddering assay for apoptosis to confirm the presence of apoptotic nucleosomal DNA fragmentation induced by p65 siRNA and HDIs (28, 29). The level of DNA fragmentation induced by the HDIs in combination with p65 siRNA significantly exceeded that observed with the agents alone ($P < 0.05$; Fig. 5B). UMSCC-11B cells were also more sensitive to the treatment than UMSCC-11A cells as measured by DNA fragmentation. These results indicate that inhibition of NF-κB by p65 siRNA sensitizes HNSCC cells to HDI-induced apoptosis.

Disruption of NF-κB by p65 siRNA Down-regulates Cell Cycle – Related Genes *p21* and *CCND1* and Anti-apoptotic Genes *IAP1* and *BCL-XL* in Response to HDIs

To explore whether HDIs and p65 siRNA have opposing effects on important genes involved in proliferation and apoptosis, we examined the effects of HDIs without or in combination with p65 siRNA on expression of *p21, cyclin D1, IAP1*, and *BCL-XL*, which are genes reported previously to regulate the cell cycle and apoptosis in HNSCC (12, 32–38). TSA induced increases in expression of *p21, cyclinD1, cIAP1*, and *BCL-XL* from baseline of differing

magnitude, kinetics, and duration (Fig. 6). p65 siRNA attenuated the increase in TSA-induced *p21* expression and significantly inhibited baseline and TSA-induced increases in *cyclin D1* and *BCL-XL* expression and, to a lesser extent, in *cIAP1* ($P < 0.05$; Fig. 6). No induction or inhibition of GAPDH to which these were normalized was observed (data not shown), indicating this was not due to nonspecific effects on global gene expression. Thus, TSA induced and p65 siRNA inhibited TSA-enhanced expression of several genes implicated in proliferation, cell survival, and oncogenesis of HNSCC, including *p21, cyclin D1, IAP1*, and *BCL-XL*.

The Proteasome Inhibitor Bortezomib and HDIs Have Combined Growth-Inhibitory Activity in UMSCC Cells

Because activation of NF-κB through degradation of IκBs is proteasome dependent (13) and we showed previously that proteasome inhibitor bortezomib is a potent pharmacologic inhibitor of NF-κB activation in human HNSCC cell lines and xenografts (14, 17, 24), we examined if bortezomib sensitized UMSCC lines and xenograft tumor to HDIs. First, we compared the effects of subtherapeutic concentrations of bortezomib (0.005 μmol/L), TSA (0.1 μmol/L), NaBu (400 μmol/L) alone and in combination on a panel of nine UMSCC cell lines by MTT assay. Figure 7A shows that treatment of cells with bortezomib, TSA, and NaBu alone at these concentrations minimally inhibited or enhanced growth of many of these UMSCC lines. However, when bortezomib was combined with HDIs, a marked decrease in cell density was observed, particularly with TSA, compared with the drugs alone ($P < 0.05$; Fig. 7A). The decrease in density was associated with cytotoxic morphologic changes similar to those observed with HDIs and p65 siRNA (data not shown).

To evaluate a potential HDI/bortezomib combination for preclinical and clinical trials, we also determined the activity of a novel hydroxamate HDI, PXD101, with bortezomib. PXD101 enhances histone acetylation and cytoxicity in tumor cells with IC_{50}s in range of 0.2 to 5 μmol/L (22) and is under investigation in phase I studies. Figure 7B shows that PXD101 (1 μmol/L) and bortezomib (0.005

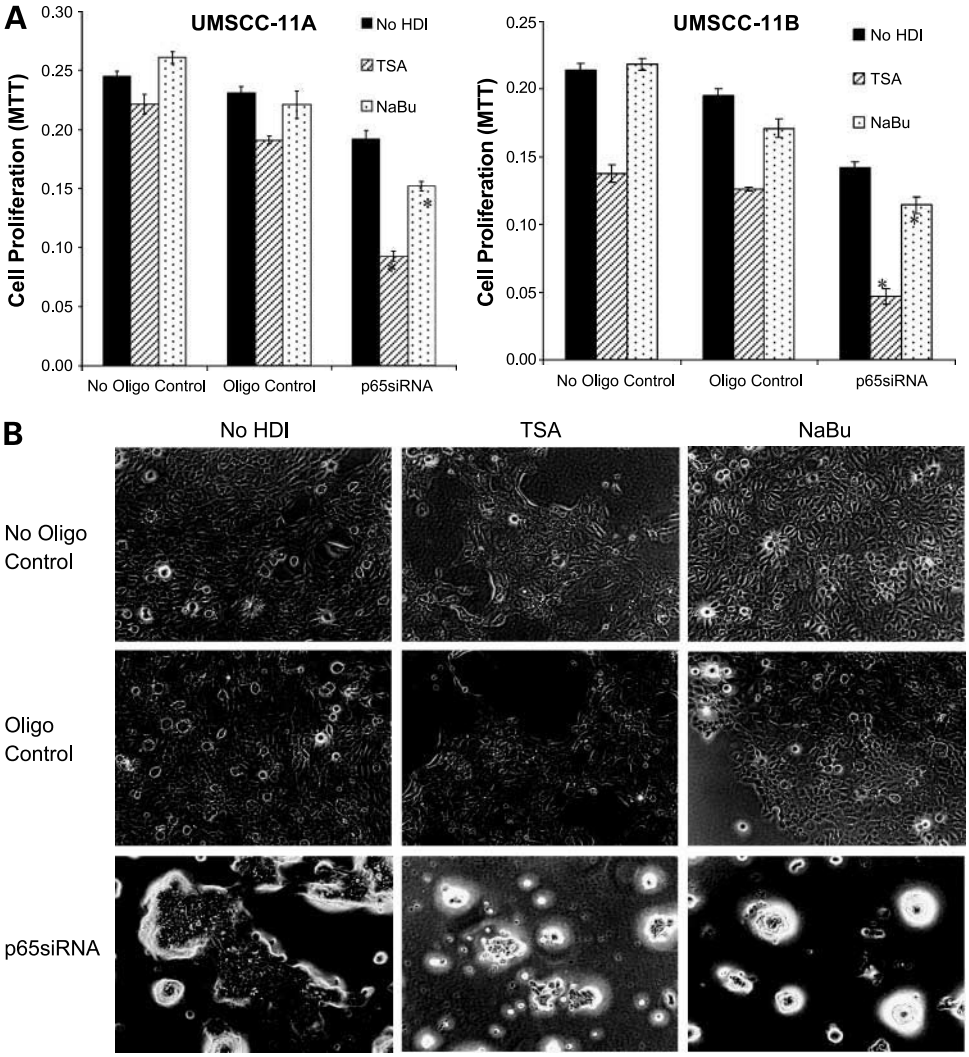

Figure 4. Inhibition of NF-κB by p65 siRNA sensitizes HNSCC to HDI. **A,** MTT assay. UMSCC-11A and UMSCC-11B cells were transfected without oligonucleotide, with oligonucleotide control, or with p65 siRNA, and TSA (0.2 μmol/L) and NaBu (500 μmol/L) were added after 24 h. The cell growth curves for 5 d were determined, and data from day 3 during optimal growth and inhibition are shown. *Columns,* mean of triplicates from two independent experiments; *bars,* SD. *, $P < 0.05$. **B,** phase-contrast photomicrographs show the effects of HDIs and p65 siRNA on cell morphology in UMSCC-11A. TSA (0.2 μmol/L) and NaBu (500 μmol/L) were added 24 h after transfection with p65 siRNA, nonspecific oligonucleotide, and no oligonucleotide control. Cells were photomicrographed at a magnification of ×100 after 48 h of TSA and NaBu treatment.

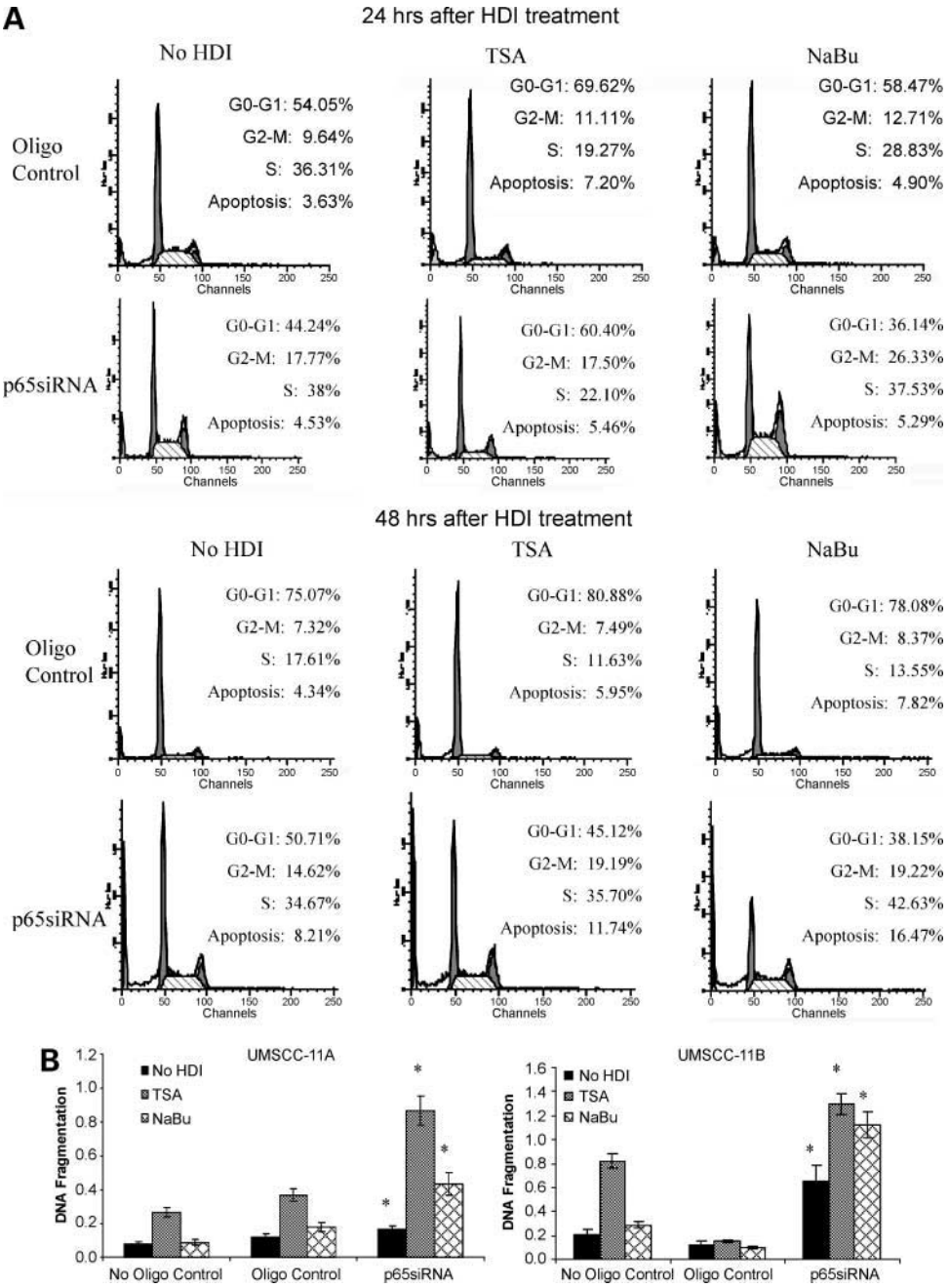

Figure 5. HDIs and p65 siRNA induce cell cycle delay, and p65 siRNA sensitizes HNSCC cells to HDI-induced apoptosis. **A,** DNA cell cycle analysis and sub–G_0-G_1 DNA fragmentation analysis were analyzed by flow cytometry. UMSCC-11A cells were transfected with p65 siRNA and oligonucleotide controls 24 h before HDIs (0.2 μmol/L TSA and 500 μmol/L NaBu) treatment. One of three independent experiments showing similar results. **B,** apoptosis DNA fragmentation assay. p65 siRNA was transfected 24 h before HDI treatment. Twenty-four hours after TSA (0.2 μmol/L) and NaBu (500 μmol/L) exposure. DNA fragmentation was confirmed and quantified using a Cell Death Detection ELISA kit. *Columns,* mean of triplicate from one of two independent experiments that showed similar results; *bars,* SD. *, $P < 0.05$.

μmol/L) alone partially inhibit growth of the UMSCC-11A cell line. In combination, strong inhibition of cell growth was observed on days 3 and 5 ($P < 0.05$). Together, these findings indicate that bortezomib can sensitize HNSCC cells to HDIs.

Combining Novel HDI PXD101 with Bortezomib Results in Greater Tumor Inhibition and Gastrointestinal Toxicity in Mice with Bortezomib-Resistant UMSCC-11A Xenografts

We next explored if PXD101 and bortezomib may have combined tumor-inhibitory activity against UMSCC-11A and/or potential toxicity *in vivo*. PXD101 has been shown to partially inhibit growth of human ovarian and colon carcinoma xenografts with minimal toxicity in mice when given daily i.p up to 40 mg/kg for 1 to 2 weeks (22). In pilot studies with PXD101 given 40, 60, and 80 mg/kg weekdays for 2 weeks, only minimal growth inhibition of bortezomib-resistant UMSCC-11A xenografts was observed at 60 and 80 mg/kg, consistent with the relative resistance of HNSCC to this agent. When PXD101 (80 mg/kg) was given daily in combination with a maximally tolerated dose of bortezomib (1 mg/kg) every 4 days, resulting diarrhea, weight,

activity loss, and deaths exceeded protocol criteria. Thus, we examined the potential antitumor activity and toxicity of combining PXD101 (60 mg/kg) weekdays for 3 weeks following pretreatment and with two additional doses of bortezomib (0.8 mg/kg) according to the schedule indicated in Fig. 7C.

Figure 7C shows that mice receiving bortezomib (0.8 mg/kg alone) showed no significant inhibition of tumor growth compared with control, consistent with our previous results showing this line and tumor is relatively bortezomib resistant in this dose range *in vivo* (14). Mice receiving PXD101 (60 mg/kg) alone showed slowed growth of tumor xenografts when compared with controls, although the differences did not reach the level of statistical significance until day 27 ($P < 0.05$) and thereafter approached growth in controls. After 1 week of treatment with the combination, significant inhibition of growth was observed at three time points ($P < 0.05$), but growth resumed during the following week and subsequently approached that of PXD101 alone and then with controls (Fig. 7C).

Increased gastrointestinal and systemic toxicity was also observed in the combination group, and to a lesser extent with PXD101, compared with the control and bortezomib groups. Increased diarrhea was observed within 3 days of start of treatment on day 13 in the combination group (three of eight) and on day 17 (two of eight); days 23, 24, and 26 (one of seven); day 30 (one of six); and day 31 (two of six); in association with lethargy days 22, 23, 24, and 29 (one of seven) and deaths on days 22 and 31 (two of eight). Delayed onset of diarrhea was noted with PXD101 alone beginning day 26 (two of eight), day 30 (one of seven), and day 31 (two of seven), with one death on day 29. No diarrhea or lethargy was observed in the control or bortezomib-only groups, with one death on day 29 in the control group of unknown cause during the same period. Correspondingly, greater weight loss was observed in the combination and PXD101 groups than in the control or bortezomib groups (data not shown). For all groups, support for increased diarrhea and weight loss was provided by supplementation with saline 2.0 mL s.c. daily and 1- to 2-day rest from PXD101 for lethargy. These results indicate that although combining this HDI and proteasome inhibitor resulted in inhibition of tumor growth, this was accompanied by gastrointestinal and systemic toxicity in this murine HNSCC xenograft model.

Discussion

Recently, HDIs have received considerable attention as potential anticancer agents for the treatment of solid and hematologic malignancies (2–5). HDIs have been shown to induce apoptosis, promote differentiation, and inhibit angiogenesis in a variety of experimental models (2–5), but it remained unclear why HDIs exhibit only modest antiproliferative and cytotoxic effects in HNSCC (6, 7). We showed previously that NF-κB is constitutively activated and contributes to cell proliferation, survival, therapeutic resistance, and angiogenesis by HNSCC (10, 11, 15–17). Increased nuclear localization of phospho-p65 has been shown in ~85% of HNSCC and associated with decreased prognosis (31). Acetylation of the p65 subunit has been implicated previously in transactivation of NF-κB, providing a potential mechanism by which HDIs could enhance the prosurvival effects of NF-κB and oppose the proapoptotic effects of HDIs (18, 19). We hypothesized that the relative resistance of HNSCC to HDIs could result from

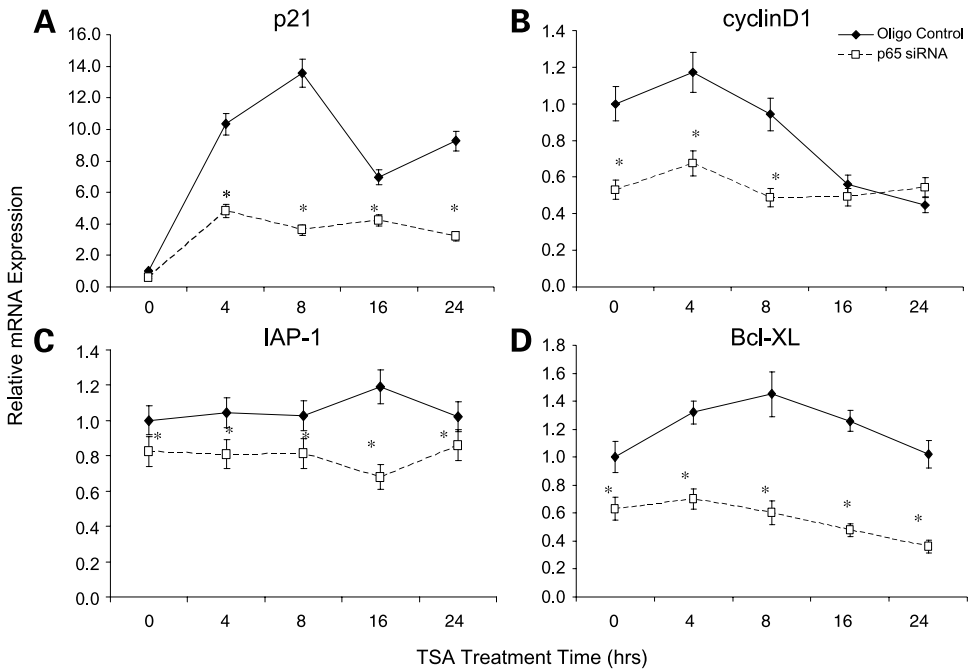

Figure 6. Inhibitory effects of p65 siRNA on constitutive and HDI-induced expression of NF-κB–regulated cell cycle–related genes *p21* and *cyclin D1* and antiapoptotic genes *IAP1* and *BCL-XL*. UMSCC-11A cells at 50% to 70% confluence were transfected with p65 (RelA) SMARTpool siRNAs (0.1 μmol/L) or control siRNA (0.1 μmol/L) for 5 h at 37°C in six-well culture plates in Opti-MEM. Twenty-four hours after transfection, cells were treated with TSA (0.2 μmol/L) and total RNAs were isolated at time points indicated. Gene expression of *p21, cyclinD1, IAP1*, and *BCL-XL* was assessed by real-time reverse transcription-PCR. GAPDH was used as the internal control. Significant inhibition by p65 siRNA compared with control. *, $P < 0.05$.

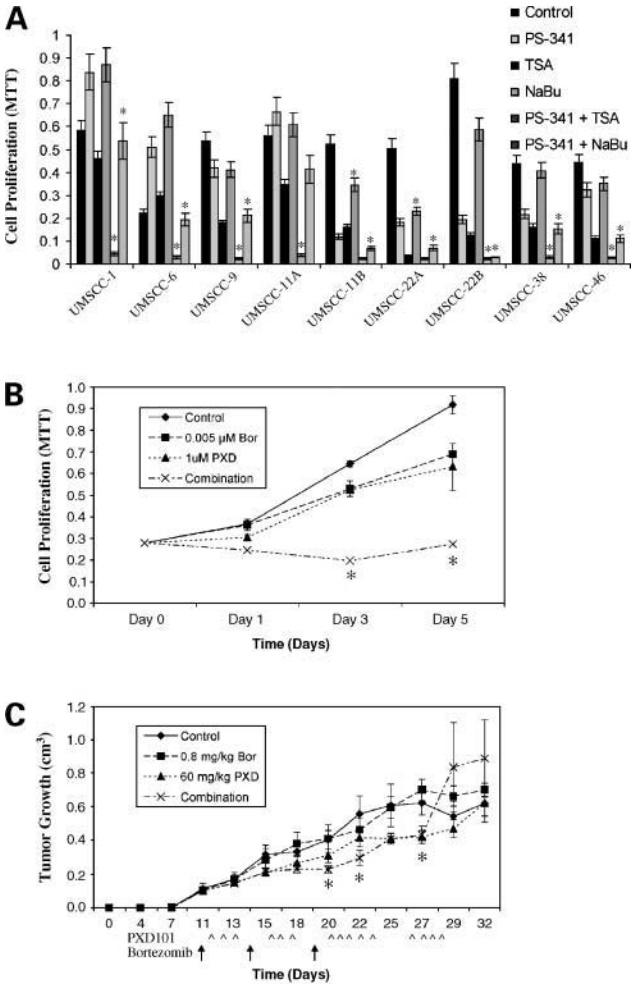

Figure 7. The proteasome inhibitor bortezomib interacts with HDIs to inhibit growth of UMSCC cells in culture and UMSCC-11A xenografts in mice. **A,** MTT assay for cell proliferation was done for a panel of nine UMSCC cell lines (UMSCC-1, UMSCC-6, UMSCC-9, UMSCC-11A, UMSCC-11B, UMSCC-22A, UMSCC-22B, UMSCC-38, and UMSCC-46) following treatment by PS-341 (0.005 μmol/L), TSA (0.1 μmol/L), NaBu (400 μmol/L) alone, and combined PS-341, TSA, or NaBu. The cell proliferation growth curves for 5 d were obtained, and data from the 3rd day are shown. *Columns,* mean of six replicates from two independent experiments; *bars,* SD. *, $P < 0.05$ (combined treatment was statistically significant when compared with single drug treatment). **B,** MTT cell proliferation assay was done for UMSCC-11A cell line following treatment by PS-341 (0.005 μmol/L), PXD101 (1 μmol/L) alone, and combined PS-341 and PXD101. The cell proliferation growth curves over 5 d were obtained. *, $P < 0.05$ (combined treatment was statistically significant when compared with single drug treatment). **C,** animals bearing established UMSCC-11A xenografts were randomized to four groups of eight mice each, to receive bortezomib alone, PXD101 alone, the combination, or no treatment, as controls. The animals in the bortezomib group and combination group received a total of three bortezomib injections (*arrows*). The animals in the PXD101 group and combination group received a total of 15 PXD101 injections over 3 wks (*open arrowheads*). The control animals received injections of normal saline and/or a L-arginine solution dissolved in PBS. *Points,* mean of eight mice per group; *bars,* SE. Saline supplementation and treatment delays were as described in Results. One animal in the combination group died on day 20. *, $P < 0.05$ indicates intervals for which combination group is significantly different from control group using Student's *t* test. Tumor size in groups treated with bortezomib or PXD101 alone did not reach statistical significance. $P > 0.05$.

the combined effects of basal and inducible activation of NF-κB and prosurvival genes. In this study, we show that HDIs enhance NF-κB transactivation, DNA binding, and acetylation of p65 in HNSCC. Specific knockdown by p65 siRNA inhibited p65 expression and p65/p50 DNA binding, enhanced the antiproliferative and cytotoxic effects of HDIs, and inhibited expression of several HDI- and NF-κB–induced cell cycle and antiapoptotic genes that are implicated in proliferation and survival of HNSCC and other cancers. Proteasome inhibitor bortezomib, which we showed previously can inhibit constitutive and inducible NF-κB activation, also sensitized HNSCC to HDIs. Consistent with the *in vitro* studies with classic HDIs, PXD101 showed limited activity in mice with UMSCC-11A xenografts resistant to bortezomib. Although combining this HDI and proteasome inhibitor produced increased antitumor activity, this was accompanied by dose-limiting gastrointestinal and systemic toxicity. Thus, low starting dosages for clinical studies combining HDIs with proteasome inhibitors and IV fluid support may be warranted.

We found that a panel of UMSCC cell lines were relatively resistant to growth inhibition by HDIs (Fig. 1A), when compared with IC_{50}s published previously for these agents (20, 21), or relative to the effects on enzymatic activity observed in HDAC assay (Fig. 1B). Increased NF-κB reporter activation was observed at these concentrations (Fig. 1C), consistent with a possible effect on NF-κB activation. The increase in NF-κB was accompanied by enhanced DNA binding of p50/p65 and acetylation of p65, implicating HDIs and enhanced acetylation in the increase in NF-κB binding and transactivation. (Fig. 2B). The activities of HDIs have been reported to include enhancement of acetylation of certain host transcription factors such as p53, E2F, and p65 RelA as well as core histones, thereby potentially resulting in complex alterations in transcription as well as chromatin structure (2–5, 18, 19, 39). Acetylation of p65 by cofactor CBP/p300 is important in transactivation and nuclear retention of NF-κB (19). Chen et al. (18) showed that the duration of nuclear NF-κB activation may be regulated by reversible acetylation of p65, and the acetylated form is subsequently deacetylated through a specific interaction with HDAC3. This deacetylation reaction promotes effective binding to IκBα and leads in turn to IκBα-dependent nuclear export of the complex through a chromosomal region maintenance-1–dependent pathway. Deacetylation of p65 by HDAC3 can thus act as an intranuclear regulatory mechanism that can control the duration of the NF-κB transcriptional response and contribute to the cytoplasmic redistribution of NF-κB–IκBα complexes. We have not excluded the possibility that HDIs enhance activation of NF-κB and cell survival through other mechanisms in addition to their affects on acetylation of p65. HDIs have also been reported to enhance NF-κB activation via upstream signal pathways. Several investigators have reported that phosphatidylinositol 3-kinase, Akt, and protein kinase C contribute to NF-κB activation by HDIs (40, 41). We have shown that phosphatidylinositol

3-kinase and Akt contribute to constitutive activation of NF-κB in HNSCC (26). Identifying the combination of upstream signal mechanisms as well as histone acetylases and HDACs important in regulating activation of NF-κB in HNSCC may provide additional targets for therapy.

Combined treatment with p65 siRNA and HDIs resulted in a clear decrease in cell density, cell cycle inhibition at G_0-G_1 and G_2-M phase, and increase in apoptosis (Figs. 4 and 5). HDI had complex effects on expression of genes important in cell cycle regulation and the downstream apoptotic cascade. The enhanced expression of *p21*, *cyclin D1*, *IAP1*, and *BCL-XL* by HDIs and inhibitory effects of p65 siRNA on their expression is consistent with a functional role for NF-κB activation in induction of these genes reported previously (33, 35–37). The accumulation of HNSCC cells in G_0-G_1 phase of the cell cycle observed with HDIs in this study are consistent with the opposing effects of *p21* and *cyclin D1* on the G_1 checkpoint. The inhibitory effect of p65 siRNA on *p21, IAP1*, and *BCL-XL* are consistent with several recent studies, which indicate that these genes can act as inhibitors of apoptosis (36, 41–45). IAP1 and BCL-XL have been shown to inhibit caspase and mitochondrial-mediated cell death (41, 42), and BCL-XL overexpression or knockdown has been shown to modulate resistance of HNSCC to apoptosis (38). Evidence indicates that p21 may attenuate HDI-mediated apoptosis due to the ability of cytoplasmic p21 to bind to and inactivate procaspase-3 (43, 44). It will be interesting to determine if abrogation of *p21* induction and the down-regulation of antiapoptotic genes, such as *BCL-XL* by p65 siRNA, contributes to the cell cycle effects and induction of apoptosis in HDI-treated HNSCC cells.

Proteasome inhibitors represent a new group of anticancer agents, which inhibit the catalytic 20S core of the proteasome, and degradation of diverse cellular proteins, including IκB, which is necessary for activation of NF-κB (13). Of the many cellular perturbations induced by proteasome inhibitors, interference with NF-κB signaling has been implicated as one of the mechanisms that contributes to their effects on proliferation, apoptosis, angiogenesis, and radiation sensitivity in SCC and other cancers (14–17, 46). Bortezomib has been approved for treatment of multiple myeloma patients who have received at least one prior therapy based on a large phase III trial (23) and is currently under investigation in clinical trials in several types of cancer (46). Bortezomib has also been shown recently to have activity in other B-cell–related malignancies, including mantle cell lymphoma, and Waldenstrom macroglobulinemia (47, 48). Evidence from preclinical and clinical studies suggest that combination with other cytotoxic therapies, or inhibitors of other prosurvival pathways, may enhance antitumor activity of bortezomib in some cancers. In preclinical and an ongoing phase I clinical study, we have found that bortezomib has NF-κB–inhibitory, antiproliferative, proapoptotic, and radiation-sensitizing activity in HNSCC (14, 17, 24). A combination, including bortezomib, gemcitabine, and carboplatinum, has shown activity and prolonged survival in patients with non–small cell lung cancer (49). Combinations with platinum or taxanes have also shown clinical responses in patients with advanced malignancies in phase I studies (50, 51).

Proteasome inhibitors have been reported to sensitize several other types of tumor cells to HDIs (52–59), but the antitumor activity and safety of such combinations *in vivo* have not been reported. The sensitizing effects of combining classic HDIs with the proteasome inhibitor bortezomib were detected in multiple UMSCC cell lines (Fig. 7A) as well as with PXD101 and bortezomib *in vitro* and *in vivo* (Fig. 7B and C). PXD101 showed limited inhibitory activity alone against UMSCC-11A proliferation and tumor growth. Bortezomib showed no inhibitory activity, consistent with the relative resistance of UMSCC-11A cells observed previously. However, combining this HDI and proteasome inhibitor was associated with gastrointestinal and systemic toxicity. Diarrhea and lethargy were also observed at a later time point in a few mice treated with PXD101 alone, suggesting that this effect may be enhanced when combined with bortezomib. Gastrointestinal toxicity and death have been reported in animal studies with higher doses of bortezomib and proteasome inhibition exceeding 90% than used in the present study. Several HDIs have been shown to have direct proteasome-inhibitory activity (55, 56), providing a possible explanation for the increased toxicity of such a combination in normal as well as malignant epithelia. NF-κB–dependent or NF-κB–independent mechanisms involving proteasome or oxidative mechanisms could contribute to antitumor activity and systemic side effects (52–58). These findings indicate that further studies of the mechanisms of activity and toxicity of proteasome and HDI inhibitors are needed. Because of the potential for enhanced toxicity, low starting dosages for clinical studies combining HDIs with proteasome inhibitors and IV fluid support may be warranted.

Acknowledgments

We thank Drs. Susan Bates and Martin Gutierrez for critical reading and comments and Drs. Xinping Yang and Ning Yeh for generous technical support.

References

1. Mao L, Hong WK, Papadimitrakopoulou VA. Focus on head and neck cancer. Cancer Cell 2004;5:311–6.

2. Jung M. Inhibitors of histone deacetylase as new anticancer agents. Curr Med Chem 2001;8:1505–11.

3. Marks PA, Richon VM, Miller T, Kelly WK. Histone deacetylase inhibitors. Adv Cancer Res 2004;91:137–68.

4. Marks PA, Dokmanovic M. Histone deacetylase inhibitors: discovery and development as anticancer agents. Expert Opin Investig Drugs 2005; 14:1497–511.

5. Marks PA, Richon VM, Rifkind RA. Histone deacetylase inhibitors: inducers of differentiation or apoptosis of transformed cells. J Natl Cancer Inst 2000;92:1210–6.

6. Gillenwater A, Xu XC, Estrov Y, Sacks PG, Lotan D, Lotan R. Modulation of galectin-1 content in human head and neck squamous carcinoma cells by sodium butyrate. Int J Cancer 1998;75:217–24.

7. Saunders N, Dicker A, Popa C, Jones S, Dahler A. Histone deacetylase inhibitors as potential anti-skin cancer agents. Cancer Res 1999; 59:399–404.

8. Coombes MM, Briggs KL, Bone JR, Clayman GL, El-Naggar AK, Dent SY. Resetting the histone code at CDKN2A in HNSCC by inhibition of DNA methylation. Oncogene 2003;22:8902 – 11.

9. Zhang Y, Jung M, Dritschilo A, Jung M. Enhancement of radiation sensitivity of human squamous carcinoma cells by histone deacetylase inhibitors. Radiat Res 2004;161:667 – 74.

10. Ondrey FG, Dong G, Sunwoo J, et al. Constitutive activation of transcription factors NF-κB, AP-1, and NF-IL6 in human head and neck squamous cell carcinoma cell lines that express pro-inflammatory and pro-angiogenic cytokines. Mol Carcinog 1999;26:119 – 29.

11. Duffey DC, Chen Z, Dong G, et al. Expression of a dominant-negative mutant inhibitor-κb-α of nuclear factor-κB in human head and neck squamous cell carcinoma inhibits survival, proinflammatory cytokine expression, and tumor growth *in vivo*. Cancer Res 1999;59:3468 – 74.

12. Loercher A, Lee TL, Ricker JL, et al. Nuclear factor-κB is an important modulator of the altered gene expression profile and malignant phenotype in squamous cell carcinoma. Cancer Res 2004;64:6511 – 23.

13. Ghosh S, May MJ, Kopp EB. NF-κB and Rel proteins: evolutionarily conserved mediators of immune responses. Annu Rev Immunol 1998;16: 225 – 60.

14. Sunwoo JB, Chen Z, Dong G, et al. Novel Proteasome inhibitor PS-341 inhibits activation of nuclear factor-κB, cell survival, tumor growth, and angiogenesis in squamous cell carcinoma. Clin Cancer Res 2001;7: 1419 – 28.

15. Duffey DC, Crowl-Bancroft CV, Chen Z, et al. Inhibition of transcription factor nuclear factor-κB by a mutant inhibitor-κBα attenuates resistance of human head and neck squamous cell carcinoma to TNF-α caspase-mediated cell death. Br J Cancer 2000;83:1367 – 74.

16. Kato T, Duffey DC, Ondrey FG, et al. Cisplatin and radiation sensitivity in human head and neck squamous carcinomas are independently modulated by glutathione and transcription factor NF-κB. Head Neck 2000;22:748 – 59.

17. Van Waes C, Sunwoo JB, DeGraff W, Mitchell JB. Radiosensitization and proteasome inhibition. In: Adams J, editor. Cancer drug discovery and development: proteasome inhibitors in cancer therapy. Totowa: Humana Press, Inc.; 2004. p. 123 – 30.

18. Chen LF, Fischle W, Verdin E, Greene WC. Duration of nuclear NF-κB action regulated by reversible acetylation. Science 2001;293:1653 – 7.

19. Chen LF, Mu Y, Greene WC. Acetylation of RelA at discrete sites regulates distinct nuclear functions of NF-κB. EMBO J 2002;21:6539 – 48.

20. Vigushin DM, Coombes RC. Histone deacetylase inhibitors in cancer treatment. Anticancer Drugs 2002;13:1 – 13.

21. Thiagalingam S, Cheng KH, Lee HJ, Mineva N, Thiagalingam A, Ponte JF. Histone deacetylases: unique players in shaping the epigenetic histone code. Ann N Y Acad Sci 2003;983:84 – 100.

22. Plumb JA, Finn PW, Williams RJ, et al. Pharmacodynamic response and inhibition of growth of human tumor xenografts by the novel histone deacetylase inhibitor PXD101. Mol Cancer Ther 2003;2:721 – 8.

23. Richardson PG, Sonneveld P, Schuster MW, et al. Bortezomib or high-dose dexamethasone for relapsed multiple myeloma. N Engl J Med 2005; 352:2487 – 98.

24. Van Waes C, Chang A, Lebowitz PF, et al. Inhibition of NF-κB and target genes during combined therapy with proteasome inhibitor botezomib and re-irradiation in patients with recurrent head and neck squamous cell carcinoma. Int J Radiat Oncol Biol Phys 2005;63:1400 – 12.

25. Krause CJ, Carey TE, Ott RW, Hurbis C, McClatchey KD, Regezi JA. Human squamous cell carcinoma. Establishment and characterization of new permanent cell lines. Arch Otolaryngol 1981;107:703 – 10.

26. Bancroft CC, Chen Z, Yeh J, et al. Effects of pharmacologic antagonists of epidermal growth factor receptor, PI3K, and MEK signal kinases on NF-κB and AP-1 activation and IL-8 and VEGF expression in human head and neck squamous cell carcinoma lines. Int J Cancer 2002; 99:538 – 48.

27. Bradford CR, Zhu S, Ogawa H, et al. P53 mutation correlates with cisplatin sensitivity in head and neck squamous cell carcinoma lines. Head Neck 2003;25:654 – 61.

28. Salgame P, Varadhachary AS, Primiano LL, Fincke JE, Muller S, Monestier M. An ELISA for detection of apoptosis. Nucleic Acids Res 1997;25:680 – 1.

29. Frankfurt OS, Krishan A. Enzyme-linked immunosorbent assay (ELISA) for the specific detection of apoptotic cells and its application to rapid drug screening. J Immunol Methods 2001;253:133 – 44.

30. Yu M, Yeh J, Van Waes C. Protein kinase casein kinase 2 mediates inhibitor-κB kinase and aberrant nuclear factor-κB activation by serum factor(s) in head and neck squamous carcinoma cells. Cancer Res 2006; 66:6722 – 31.

31. Zhang PL, Pellitteri PK, Law A, et al. Overexpression of phosphorylated nuclear factor-κB in tonsillar squamous cell carcinoma and high-grade dysplasia is associated with poor prognosis. Mod Pathol 2005;18:924 – 32.

32. Mobley SR, Liu TJ, Hudson JM, Clayman GL. *In vitro* growth suppression by adenoviral transduction of p21 and p16 in squamous cell carcinoma of the head and neck: a research model for combination gene therapy. Arch Otolaryngol Head Neck Surg 1998;124:88 – 92.

33. Basile JR, Eichten A, Zacny V, Munger K. NF-κB-mediated induction of p21(Cip1/Waf1) by tumor necrosis factor α induces growth arrest and cytoprotection in normal human keratinocytes. Mol Cancer Res 2003;1: 262 – 70.

34. Sauter ER, Nesbit M, Litwin S, Klein-Szanto AJP, Cheffetz S, Herlyn M. Antisense cyclin D1 induces apoptosis and tumor shrinkage in human squamous carcinomas. Cancer Res 1999;59:4876 – 81.

35. Guttridge DC, Albanese C, Reuther JY, Pestell RG, Baldwin AS, Jr. NF-κB controls cell growth and differentiation through transcriptional regulation of cyclin D1. Mol Cell Biol 1999;19:5785 – 99.

36. Wang C-Y, Mayo MW, Korneluk RG, Goeddel DV, Baldwin AS, Jr. NF-κB antiapoptosis: induction of TRAF1 and TRAF2 and c-IAP1 and c-IAP2 to suppress caspase-8 activation. Science 1998;281:1680 – 3.

37. Chen C, Edelstein LC, Gelinas C. The Rel/NF-κB family directly activates expression of the apoptosis inhibitor Bcl-x(L). Mol Cell Biol 2000; 20:2687 – 95.

38. Bauer JA, Trask DK, Kumar B, et al. Reversal of cisplatin resistance with a BH3 mimetic, (−)-gossypol, in head and neck cancer cells: role of wild-type p53 and Bcl-xL. Mol Cancer Ther 2005;4:1096 – 104.

39. Mayo MW, Denlinger CE, Broad RM, et al. Ineffectiveness of histone deacetylase inhibitors to induce apoptosis involves the transcriptional activation of NF-κB through the Akt Pathway. J Biol Chem 2003;278: 18980 – 9.

40. Denlinger CE, Rundall BK, Jones DR. Inhibition of phosphatidylinositol 3-kinase/Akt and histone deacetylase activity induces apoptosis in non-small cell lung cancer *in vitro* and *in vivo*. J Thorac Cardiovasc Surg 2005;130:1422 – 9.

41. Xueli F, Yingwang L, Jason JC. Down-regulation of p21 contributes to apoptosis induced by HPV E6 in human mammary epithelial cells. Apoptosis 2005;10:63.

42. Gartel AL, Tyner AL. The role of the cyclin-dependent kinase inhibitor p21 in apoptosis. Mol Cancer Ther 2002;1:639 – 49.

43. Asada M, Yamada T, Ichijo H, et al. Apoptosis inhibitory activity of cytoplasmic p21(Cip1/WAF1) in monocytic differentiation. EMBO J 1999; 18:1223 – 34.

44. Rosato RR, Almenara JA, Yu C, Grant S. Evidence of a functional role for p21WAF1/CIP1 down-regulation in synergistic antileukemic interactions between the histone deacetylase inhibitor sodium butyrate and flavopiridol. Mol Pharmacol 2004;65:571 – 81.

45. Bai J, Sui J, Demirjian A, Vollmer CM, Jr., Marasco W, Callery MP. Predominant Bcl-XL knockdown disables antiapoptotic mechanisms: tumor necrosis factor-related apoptosis-inducing ligand-based triple chemotherapy overcomes chemoresistance in pancreatic cancer cells *in vitro*. Cancer Res 2005;65:2344 – 52.

46. Van Waes C. NF-κB in pathogenesis, prevention and therapy of cancer. Clin Cancer Res. In press 2007.

47. O'Connor OA, Wright J, Moskowitz C, et al. Phase II clinical experience with the novel proteasome inhibitor bortezomib in patients with indolent non-Hodgkin's lymphoma and mantle cell lymphoma. J Clin Oncol 2005;23:676 – 84.

48. Chen CI, Kouroukis T, White D, et al. Bortezomib is active in Waldenstrom's macroglobulinemia—results of a National Cancer Institute of Canada phase II study in previously untreated WM. J Clin Oncol Suppl 2006;24:432s, 7543.

49. Lara PN, Gumerlock, PH, Crowley J, Gandara DR. Bortezomib and gemcitabine/carboplatin results in encouraging survival in advanced non-small cell lung cancer: results of a phase II Southwest oncology group trial (SO339). J Clin Oncol Suppl 2006;24:368s, 7017.

50. Aghajanian C, Dizon DS, Sabbatini P, Raizer JJ, Dupont J, Spriggs DR. Phase I trial of bortezomib and carboplatin in recurrent ovarian or primary peritoneal cancer. J Clin Oncol 2005;23:5943 – 9.

51. Ma C, Mandrekar SJ, Alberts SR, et al. A phase I and pharmacologic study of sequences of the proteasome inhibitor, bortezomib (PS-341, Velcade), in combination with paclitaxel and carboplatin in patients with advanced malignancies. Cancer Chemother Pharmacol. In press 2007.

52. Denlinger CE, Keller MD, Mayo MW, Broad RM, Jones DR. Combined proteasome and histone deacetylase inhibition in non-small cell lung cancer. J Thorac Cardiovasc Surg 2004;127:1078 – 86.

53. Denlinger CE, Rundall BK, Jones DR. Proteasome inhibition sensitizes non-small cell lung cancer to histone deacetylase inhibitor-induced apoptosis through the generation of reactive oxygen species. J Thorac Cardiovasc Surg 2004;128:740 – 8.

54. Pei XY, Dai Y, Grant S. Synergistic induction of oxidative injury and apoptosis in human multiple myeloma cells by the proteasome inhibitor bortezomib and histone deacetylase inhibitors. Clin Cancer Res 2004;10: 3839 – 52.

55. Catley L, Weisberg E, Tai YT, et al. NVP-LAQ824 is a potent novel histone deacetylase inhibitor with significant activity against multiple myeloma. Blood 2003;102:2615 – 22.

56. Yin L, Laevsky G, Giardina C. Butyrate suppression of colonocyte NF-κB activation and cellular proteasome activity. J Biol Chem 2001;276: 44641 – 6.

57. Dai Y, Rahmani M, Dent P, Grant S. Blockade of histone deacetylase inhibitor-induced RelA/p65 acetylation and NF-κB activation potentiates apoptosis in leukemia cells through a process mediated by oxidative damage, XIAP downregulation, and c-Jun N-terminal kinase 1 activation. Mol Cell Biol 2005;25:5429 – 44.

58. Takada Y, Gillenwater A, Ichikawa H, Aggarwal BB. Suberoylanilide hydroxamic acid potentiates apoptosis, inhibits invasion, and abolishes osteoclastogenesis by suppressing nuclear factor-κB activation. J Biol Chem 2006;281:5612 – 22.

59. Hu J, Colburn NH. Histone deacetylase inhibition down-regulates cyclin D1 transcription by inhibiting nuclear factor-κB/p65 DNA binding. Mol Cancer Res 2005;3:100 – 9.

Molecular Cancer Therapeutics

Nuclear factor-κB p65 small interfering RNA or proteasome inhibitor bortezomib sensitizes head and neck squamous cell carcinomas to classic histone deacetylase inhibitors and novel histone deacetylase inhibitor PXD101

Jianming Duan, Jay Friedman, Liesl Nottingham, et al.

Mol Cancer Ther 2007;6:37-50.